



Received 14 May 2018
Accepted 12 September 2018

Edited by G. Kostorz, ETH Zurich, Switzerland

Keywords: TOPAS macros; whole powder pattern modelling; WPPM; powder diffraction.

Supporting information: this article has supporting information at journals.iucr.org/j

Whole powder pattern modelling macros for TOPAS

Paolo Scardi,^{a*} Cristy L. Azanza Ricardo,^b Camilo Perez-Demydenko^{a,c} and Alan A. Coelho^d

^aDepartment of Civil, Environmental and Mechanical Engineering, University of Trento, Via Mesiano 77, 38123 Trento, Italy, ^bCentro de Física Aplicada y Tecnología Avanzada, Universidad Nacional Autónoma de México, Boulevard 14 Juriquilla 3001, Santiago de Querétaro, Qro., 76230, Mexico, ^cInstitute of Materials Science and Technology (IMRE) – Physics Faculty, University of Havana, Zapata y G, 10400 Havana, Cuba, and ^d72 Cedar Street, Wynnum, Brisbane, Australia. *Correspondence e-mail: paolo.scardi@unitn.it

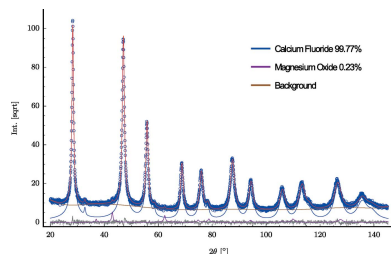
Macros implementing the main concepts of the whole powder pattern modelling approach have been written for TOPAS. Size and strain broadening components of the diffraction line profiles can be convolved with the instrumental profile already available among the standard commands of TOPAS. Specific macros are presented with examples of applications including plastically deformed powders and atomistic simulations. A macro is presented for the modelling of surface relaxation effects in spherical nanocrystals.

1. Introduction

Line profile analysis (LPA) is commonly used in diffraction for the microstructural characterization of powder and polycrystalline materials. The main information concerns the shape and size of the coherent diffraction domains (also referred to as crystallites), mistakes in the stacking sequence of atomic layers, and inhomogeneous atomic displacement caused by defects like, for example, dislocations, grain–grain interaction in polycrystalline aggregates or surface relaxation of nanocrystals (Snyder *et al.*, 1999; Mittemeijer & Scardi, 2003).

Interest in LPA extends to structural studies, where an accurate description of the line profile is necessary to obtain reliable values of intensity and peak positions from the powder patterns (McCusker *et al.*, 1999). This further motivation has led, in the past two decades, to a growing integration of LPA into Rietveld refinement codes, which today provide for a more sophisticated treatment of the line profile than in the original method (Rietveld, 1967, 1969; Young, 1995). The need for a better integration of structure–microstructure analysis is the motivation of the present work, where we propose specific macros for TOPAS (Coelho, 2017, 2018), one of the most popular and powerful software tools for powder diffraction data analysis. The theory and methods are directly taken from the whole powder pattern modelling (WPPM) approach (see Scardi, 2008, and references therein) but, differently from most WPPM applications where peak intensities are treated as free parameters, LPA implementations in this work are subject to the structural constraints of the Rietveld method.

To allow the use of LPA under the most varied conditions, we have limited our attention to models of general validity. In particular, our treatment of broadening from crystallite size is based on the hypothesis of spherical domain shape. This is a



© 2018 International Union of Crystallography

reasonable approximation for many practical cases, with the advantage of not having to consider the unit-cell orientation. Size dispersion is accounted for by a lognormal distribution of diameters, which is also a rather flexible and commonly used solution; different distributions can be easily implemented following the same approach and existing literature. Concerning the effect of inhomogeneous strain (so-called microstrain), we describe a routine applicable to any crystal symmetry, based on the Laue class of the studied phases, for two frequently recurring cases:

(i) Study of dislocations, according to the Krivoglaz-Wilkens theory (Krivoglaz & Ryaboshapka, 1963; Krivoglaz *et al.*, 1983; Wilkens, 1969*a,b*, 1970). Given the contrast factor for the specific elastic medium and dislocation slip system and character (Kužel & Klimanek, 1988; Martinez-Garcia *et al.*, 2009), the procedure gives an average dislocation density and an effective outer cut-off radius.

(ii) Implementation of a general microstrain model, called PAH, that is flexible enough to adapt to most cases where an inhomogeneous strain has visible and anisotropic effects on the line profile. Results are presented as Warren plots (Warren & Averbach, 1950), as shown in more detail below.

A further TOPAS macro is presented for the effect of surface relaxation in nanocrystals of spherical shape, according to a method recently published (Perez-Demydenko

& Scardi, 2017). The latter constitutes the first example of peak asymmetry modelling using the imaginary Fourier transform strain component in the framework of the WPPM approach. Case studies are briefly reported to demonstrate the application of the macros.

2. WPPM TOPAS macros: theory

2.1. Size broadening for spherical domains

The size broadening effect is modelled assuming spherical crystalline domains with a lognormal distribution of diameters, D (Langford *et al.*, 2000; Scardi, 2008):

$$g(D) = \frac{1}{D\sigma(2\pi)^{1/2}} \exp\left[-\frac{1}{2}\left(\frac{\ln D - \mu}{\sigma}\right)^2\right], \quad (1)$$

where μ and σ are the lognormal mean and variance, respectively. It is relatively straightforward to change the distribution, if necessary, for example for a Gamma distribution (Scardi & Leoni, 2001); it is also possible to use a different – virtually any (Leonardi *et al.*, 2012) – domain shape, although for non-spherical shapes the orientation of the unit cell should be specified. For the sake of simplicity and generality, here we consider the spherical shape, leaving

```
macro WPPM_Sphere_LogNormDIST(muc, muv, sigc, sigv)
{
    #m_argu muc
    #m_argu sigc
    If_Prm_Eqn_Rpt(muc, muv, min .1 max = Min(2 Val + .3, 100;))
    If_Prm_Eqn_Rpt(sigc, sigv, min .01 max = Min(2 Val + .01, 3;))
    WPPM_ft_conv =
    {
        def u = CeV(muc, muv);
        def sig = CeV(sigc, sigv);
        fn M(n) = 0.5 Exp(- n (u + (3 - 0.5 n) sig^2));
        fn wppm_Ln(kc) = Get(WPPM_Ln_k) + Ln(kc Get(WPPM_dL));
        fn q(n) {
            return
                Erfc_Approx( ( wppm_Ln(1) - u - (3-n) sig^2) / (sig Sqrt(2)))
                WPPM_L^n
                M(n);
        }
        return q(0) - 1.5 q(1) + 0.5 q(3);
    }
    WPPM_break_on_small = 1e-7;
    WPPM_L_max 1000
    WPPM_th2_range = 30;
}
```

Figure 1

TOPAS macro WPPM_Sphere_LogNormDIST, for the line profile component due to the finite size of the crystalline domains, assumed to be spherical with a lognormal distribution of diameters.

```
WPPM_Sphere_LogNormDIST(mu, 2.3, sigma, 0.5)
prm !AverageDiameter = Exp(mu+sigma^2/2); : 11.2
prm !StanDev = (Exp(2*mu+sigma^2)*(Exp(sigma^2)-1))^(1/2); : 5.7
```

Figure 2

Macro call example for macro WPPM_Sphere_LogNormDIST.

computer programs

```

macro WPPM_Strain_InvariantWilkins(rhoc, rhov, Rec, Rev, burgers, wsg, E1, E2, E3,
E4, E5, E6, E7, E8, E9, E10, E11, E12, E13, E14, E15)
{
    #m_argu rhoc
    #m_argu Rec
    If_Prm_Eqn_Rpt(rhoc, rhov, min 0 max = Min(2 Val + .0001, 0.100););
    If_Prm_Eqn_Rpt(Rec , Rev , min 1 max = Min(2 Val + .0001, 0.100;);

    WPPM_ft_conv = {
        def invariantTerm_0 = getInvariant(wsg, E1, E2, E3, E4, E5, E6, E7, E8, E9,
        E10, E11, E12, E13, E14, E15);
        def invariantTerm = If (invariantTerm_0 < 0, 1000, invariantTerm_0);
        def dstar = 1/(D_spacing 0.1);
        def aa = Constant(Get(a) 0.1);
        def strainINV = invariantTerm/((aa dstar)^4);
        def rhoVal = CeV(rhoc, rhov);
        def fact = Pi burgers burgers rhoVal dstar dstar strainINV 0.01 0.5;
        def Reval = CeV(Rec, Rev);
        def eta = Abs(WPPM_L/Reval);
        def fstar = If ( eta < 1, -Ln(eta) + 7/4 - Ln(2) + eta*eta/6 -
        (32*eta*eta)/(225*Pi), 256.0/(45.0*Pi*eta)-(11.0/24.0 +
        (Ln(2)+Ln(eta))/4.0)/(eta*eta));
        def result = If (WPPM_L == 0, 1, Exp(-fact*(WPPM_L*WPPM_L*fstar)));
        return result;
    }
    WPPM_break_on_small = 1e-7;
    WPPM_L_max 1000
    WPPM_th2_range = 30;
}

```

Figure 3

TOPAS macro `WPPM_Strain_InvariantWilkins`, for the line profile component due to the inhomogeneous strain of dislocations.

extensions to other shapes to future work; however, macros for some additional shapes are already available.

The spherical shape is implemented by the corresponding Fourier transform (FT) of the line profile (Wilson, 1962), which can be generalized to the case of a distribution of diameters as (Scardi, 2008)

$$A(L) = q_0(L) - \frac{3}{2}q_1(L) + \frac{1}{2}q_3(L). \quad (2)$$

Here, L is the Fourier length, *i.e.* the distance between any two scatterers along the scattering vector direction, and

$$q_n(L) = M_n L^n \operatorname{erfc} \left[\frac{\ln L - \mu - (3-n)\sigma^2}{\sigma(2)^{1/2}} \right]. \quad (3)$$

M_n is related to the moments of the lognormal distribution and is defined as

$$M_n = \frac{1}{2} \exp \{-n[\mu + (3-n/2)\sigma^2]\}. \quad (4)$$

The corresponding *TOPAS* macro `WPPM_Sphere_LogNormDIST`(*muc*, *muv*, *sigc*, *sigv*) (see Fig. 1¹)

¹ To use this and all the following macros, it is suggested to not copy the text in the figures but to download the file `WPPM_macros.inc` from the supplementary information files and copy it into the folder where you keep the input file you need to use; then, add to the input files a command `#include WPPM_macros.inc`. As an alternative, check the `TOPAS.inc` file. If the macros are already present in your release of *TOPAS* (7 and higher), then you do not have to add the `#include` command; otherwise you might copy all of the text in `WPPM_macros.inc` and paste it at the bottom of the `Topas.inc` file.

involves two refinable parameters, μ and σ , from which the mean diameter ($\langle D \rangle$) and standard deviation of the distribution (s.d.) can be obtained as

$$\langle D \rangle = \exp(\mu + \sigma^2/2), \quad (5a)$$

$$\text{s.d.} = \{\exp(2\mu + \sigma^2)[\exp(\sigma^2) - 1]\}^{1/2}. \quad (5b)$$

Then, a complete call to this macro can be structured as in Fig. 2. The variability range of the parameters can be limited by `min` and `max` functions. Suggested limits for μ are from 0.1 to the smaller between twice the current value plus 0.3 and 100; similarly, σ can be restricted between 0.01 and the smaller between twice the current value plus 0.01 and 3.

2.2. Anisotropic strain broadening

Strain broadening is implemented in two macros: (i) `WPPM_Strain_InvariantWilkins` (Fig. 3) and (ii) `WPPM_Strain_InvariantPAH` (Fig. 4). While the former is based on the Krivoglaz–Wilkins theory for dislocation line broadening (Krivoglaz & Ryaboshapka, 1963; Krivoglaz *et al.*, 1983; Wilkins, 1969*a,b*, 1970) generalized to any crystal system (Martinez-Garcia *et al.*, 2009), the latter is a flexible (adaptive) approach based on the phenomenological observations of Adler & Houska (1979), extended according to the approach of Stokes & Wilson (1944) and Popa (1998), respectively, for cubic materials and for any crystal system.

Table 1

Number of invariant coefficients according to the Laue class of the studied phase.

Laue class	$\bar{1}$	$2/m$	Mmm	$4/m$	$4/mmm$	$\bar{3}$	$\bar{3}m$	$6/m, 6/mmm$	$m\bar{3}, m\bar{3}m$
Space groups	1–2	3–15	16–74	75–88	89–142	143–148	149–167	168–194	195–230
No. of independent E_i terms	15	9	6	5	4	5	4	3	2

Both models are based on the general expression of the FT of the strain broadening effect, related to the root mean square strain for a distance L along $[hkl]$ (also termed the microstrain), $\langle \varepsilon_{hkl}^2 \rangle^{1/2}$, as (Warren, 1990)

$$A_{hkl}^D(L) = \exp\left[(-2\pi^2 L^2/d_{hkl}^2)\langle \varepsilon_{hkl}^2(L) \rangle\right], \quad (6)$$

where d_{hkl} is the interplanar distance.

In the case of the `WPPM_Strain_InvariantWilkins` macro, according to Wilkins (1969a,b, 1970) the microstrain can be written as

$$\langle \varepsilon_{hkl}^2(L) \rangle = \frac{\rho b^2}{4\pi} \Gamma_{hkl} f^*(L/R_e), \quad (7)$$

where $f^*(L/R_e)$ is the so-called Wilkins function [see Wilkins (1969a,b) for details], giving the appropriate decay to the FT for increasing L ; ρ is the average dislocation density, R_e is the effective outer cut-off radius of the dislocation strain field, b is the modulus of the Burgers vector of the given dislocation system and Γ_{hkl} is the average contrast factor of this system, which encodes the main part of the anisotropic broadening effect (Wilkins, 1969a,b; Martinez-Garcia *et al.*, 2009) [a more complete formulation is discussed by Armstrong *et al.* (2006)].

As shown on rather general grounds by Popa (1998), the anisotropy of microstrain can be described by an invariant form, expressed as a fourth-order polynomial of the Miller indices:

$$\langle \varepsilon_{hkl}^2(L) \rangle = (d_{hkl}^4/a^4)\Gamma_{hkl}, \quad (8)$$

where

$$\begin{aligned} \Gamma_{hkl} = & E_1 h^4 + E_2 k^4 + E_3 l^4 + 2(E_4 h^2 k^2 + E_5 k^2 l^2 + E_6 h^2 l^2) \\ & + 4(E_7 h^3 k + E_8 h^3 l + E_9 k^3 h + E_{10} k^3 l + E_{11} l^3 h + E_{12} l^3 k) \\ & + 4(E_{13} h^2 k l + E_{14} k^2 h l + E_{15} l^2 h k) \end{aligned} \quad (9)$$

and a is the lattice parameter. The number of independent E_i coefficients in the invariant is related to point symmetry rules, ranked according to the Laue class (Table 1). Given the space-group number (`sg`) and the corresponding number of independent E_i , the macro `getInvariant` (see Fig. 5) returns the resultant form of equation (9).

The `WPPM_Strain_InvariantWilkins` macro requires starting values of average dislocation density and effective cut-off radius, in addition to the modulus of the Burgers vector of the slip system, the space-group number of the studied material and the number of invariant coefficients for the given symmetry. Fig. 6 shows an example of application to a face-centred cubic metal, requiring just two terms in the invariant form, E_1 and E_4 , whereas the Burgers vector modulus (burgers) is related to the unit-cell parameter (a_0).

In Fig. 6, `rho` (ρ) is in units of nm^{-2} (10^{18} m^{-2}) and `re` (R_e) is in nm. Values of ρ larger than 0.1 nm^{-2} are unphysical, whereas typically the technique is not sensitive to dislocation effects for $\rho < 0.0001 (\times 10^{18} \text{ m}^{-2})$. Concerning R_e , the values

```
macro WPPM_Strain_InvariantPAH(ac, av, bc, bv, wsg, E1, E2, E3, E4, E5, E6, E7, E8,
E9, E10, E11, E12, E13, E14, E15)
{
    #m_argu ac
    #m_argu bc
    If_Prm_Eqn_Rpt(ac, av, min 0 max = Min(2 Val + .0001, 0.100););
    If_Prm_Eqn_Rpt(bc, bv, min 0 max = Min(2 Val + .0001, 0.100););
    WPPM_ft_conv = {
        def invariantTerm_0 = getInvariant(wsg, E1, E2, E3, E4, E5, E6, E7, E8, E9,
        E10, E11, E12, E13, E14, E15);
        def invariantTerm = If (invariantTerm_0 < 0, 1000, invariantTerm_0);
        def dstar = 1/(D_spacing*0.1);
        def aa = Constant(Get(a) 0.1);
        def strainINV = invariantTerm/((aa*dstar)^4);
        def fact = 2*Pi*Pi*dstar*dstar*strainINV;
        def aVal = CeV(ac, av)*1e-5;
        def bVal = CeV(bc, bv)*1e-5;
        return Exp(-fact*(aVal*WPPM_L+bVal*WPPM_L*WPPM_L));
    }
    WPPM_break_on_small = 1e-7;
    WPPM_L_max 1000
    WPPM_th2_range = 30;
}
```

Figure 4

`TOPAS` macro `WPPM_Strain_InvariantPAH`, a microstrain line broadening model based on a phenomenological expression.

computer programs

should be limited by the maximum domain size for randomly distributed (little interacting) dislocations, while small values, even unity and below, can indicate strong interaction, like in dipoles and grain boundary structures (Wilkins, 1970). So it makes sense to limit R_e between 0.1 and the maximum D value (or 500 nm, which is a sufficiently long distance for an upper

limit to line profile effects). More details on the meaning of R_e and ρ , and on the applicability of the Wilkins model to nanocrystalline materials, are given by Leonardi & Scardi (2015, 2016).

Given the slip system and the elastic tensor, the E_i coefficients can be calculated (Martinez-Garcia *et al.*, 2009);

```
macro getInvariant(sg, E1, E2, E3, E4, E5, E6, E7, E8, E9, E10, E11, E12, E13, E14,
E15)
{
    #if Or(sg == 1, sg == 2); 'Triclinic, -1
    E1*H^4 + E2*K^4 + E3*L^4 + 2*(E4*H*K*K + E5*K*K*L*L + E6*H*H*L*L) +
    4*(E7*(H^3)*K + E8*(H^3)*L + E9*H*(K^3) + E10*(K^3)*L + E11*H*(L^3) +
    E12*K*(L^3) + E13*H*H*K*L + E14*H*K*K*L + E15*H*K*L*L)

    #elseif And(sg >= 3, sg <= 15); 'Monoclinic, 2/m
    If (And(Constant(Get(al)) == 90, Constant(Get(ga)) == 90), ' unique axis b
        E1*H^4 + E2*K^4 + E3*L^4 + 2*(E4*H*H*L*L + E5*K*K*L*L + E6*H*H*K*K) +
        4*(E7*(H^3)*L + E8*H*(L^3) + E9*H*K*K*L),
        If (And(Constant(Get(al)) == 90, Constant(Get(be)) == 90), ' unique axis c
            E1*H^4 + E2*K^4 + E3*L^4 + 2*(E4*H*H*K*K + E5*K*K*L*L +
            E6*H*H*L*L) + 4*(E7*(H^3)*K + E8*H*(K^3) + E9*H*K*L*L),
            "Invalid Monoclinic lattice parameters"
        )
    )

    #elseif And(sg >= 16, sg <= 74); 'Orthorhombic, mmm
    E1*H^4 + E2*K^4 + E3*L^4 + 2*(E4*H*H*K*K + E5*K*K*L*L + E6*H*H*L*L)

    #elseif And(sg >= 75, sg <= 88); 'Tetragonal, 4/m
    E1*(H^4 + K^4) + E2*L^4 + 2*E3*H*H*K*K + 2*E4*(H*H + K*K)*L*L +
    4*E5*H*K*(H*H - K*K)

    #elseif And(sg >= 89, sg <= 142); 'Tetragonal, 4/mmm
    E1*(H^4 + K^4) + E2*L^4 + 2*E3*H*H*K*K + 2*E4*(H*H + K*K)*L*L

    #elseif And(sg >= 143, sg <= 148); 'Trigonal, -3
    #if Or(sg == 146, sg == 148); 'Trigonal space groups supporting
    'also rhombohedral axes
    If (Constant(Get(ga)) == 120,
        E1*(H*H - H*K + K*K)^2 + 2*E2*(H*H - H*K + K*K)*L*L + E3*L^4 +
        4*E5*(H^3 - 3*H*K*K + (K^3))*L + 4*E4*H*(H - K)*K*L,
        If (Constant(Get(ga)) == 60,
            E1*(H*H + H*K + K*K)^2 + 2*E2*L*L*(H*H + H*K + K*K) +
            E3*L^4 + (4/3)*E4*L*(H^3 + 3*H*H*K - K^3) +
            (4/3)*E5*L*(-H^3 + 3*H*K*K + K^3), ' 60deg
            E1*(H^4 + K^4 + L^4) + 2*E2*(H*H*K*K + H*H*L*L +
            K*K*L*L) + 4*E3*((H^3)*K + (K^3)*L + H*(L^3)) +
            *E4*(H*(K^3) + (H^3)*L + K*(L^3)) + 4*E5*H*K*L*(H + K + L)
        )
    )
    #else
    If (Constant(Get(ga)) == 120,
        E1*(H*H - H*K + K*K)^2 + 2*E2*(H*H - H*K + K*K)*L*L + E3*L^4 +
        4*E5*(H^3 - 3*H*K*K + (K^3))*L + 4*E4*H*(H - K)*K*L,
        E1*(H*H + H*K + K*K)^2 + 2*E2*L*L*(H*H + H*K + K*K) + E3*L^4 +
        (4/3)*E4*L*(H^3 + 3*H*H*K - K^3) + (4/3)*E5*L*(-H^3 + 3*H*K*K + K^3) ' 60
    )
    #endif
}
```

Figure 5

TOPAS macro `getInvariant`, providing Popa's invariant according to the space group (part 1 of 2).

approximate parametric expressions are available for cubic systems (Ungár *et al.*, 1999; Dragomir & Ungár, 2002). If the dislocation slip system is undetermined the invariant coefficients can be refined by the *TOPAS* macro. However, when freely adjusting the coefficients, it is important to

consider that negative values of the invariant form of equation (9) make no sense (Popa, 1998). To guarantee positivity, a strong condition was set on the invariant, imposing a very high value of the invariant when the refinement leads to a negative value:

```

#elseif And(sg >= 149, sg <= 167); 'Trigonal, -3m
  #if Or(sg ==150, sg ==152, sg ==154, sg ==155, sg ==156, sg ==158,
  sg ==160, sg ==161, sg ==164, sg ==165, sg ==166, sg ==167); 'Trigonal, -3m1
    #if Or(sg == 155, sg == 160, sg == 161, sg == 166, sg == 167); 'Trigonal
      'space groups supporting also rhombohedral axes
      If (Constant(Get(ga)) == 120,
        E1*(H*H - H*K + K*K)^2 + 2*E2*L*L*(H*H - H*K + K*K) + E3*L^4
        + 4*E4*H*K*L*(H - K),
        If (Constant(Get(ga)) == 60,
          E1*(H*H + H*K + K*K)^2 + 2*E2*L*L*(H*H + H*K + K*K) +
          E3*L^4 + 4*E4*H*K*L*(H + K), ' 60deg
          E1*(H^4 + K^4 + L^4) + 2*E2*(H*H*K*K + H*H*L*L +
          K*K*L*L) + 4*E3*(H*K*(H*H + K*K) + H*L*(H*H + L*L) +
          K*L*(K*K + L*L)) + 4*E4*H*K*L*(H + K + L)
        )
      )
    #else
      If (Constant(Get(ga)) == 120,
        E1*(H*H - H*K + K*K)^2 + 2*E2*L*L*(H*H - H*K + K*K) + E3*L^4
        + 4*E4*H*K*L*(H - K),
        E1*(H*H + H*K + K*K)^2 + 2*E2*L*L*(H*H + H*K + K*K) + E3*L^4
        + 4*E4*H*K*L*(H + K) ' 60deg
      )
    #endif
  #else 'Trigonal, -31m
    If (Constant(Get(ga)) == 120,
      E1*(H*H - H*K + K*K)^2 + 2*E2*L*L*(H*H - H*K + K*K) + E3*L^4
      + E4*L*(4*(H^3) - 6*H*H*K - 6*H*K*K + 4*(K^3)),
      E1*(H*H + H*K + K*K)^2 + 2*E2*L*L*(H*H + H*K + K*K) + E3*L^4
      + (4/3)*E4*L*(2*(H^3) + 3*H*H*K - 3*H*K*K - 2*(K^3)) ' 60deg
    )
  #endif

#elseif And(sg >= 168, sg <= 194); 'Hexagonal, 6/m and 6/mmm
  If (Constant(Get(ga)) == 120,
    E1*(H*H - H*K + K*K)^2 + 2*E2*L*L*(H*H - H*K + K*K) + E3*L^4,
    E1*(H*H + H*K + K*K)^2 + 2*E2*L*L*(H*H + H*K + K*K) + E3*L^4 ' 60deg
  )

#elseif And(sg >= 195, sg <= 230); 'Cubic, m-3 and m-3m
  E1*(H^4 + K^4 + L^4) + 2*E2*(H*H*K*K + H*H*L*L + K*K*L*L)

#else
#endif
}

```

Figure 5 (continued)

TOPAS macro `getInvariant`, providing Popa's invariant according to the space group (part 2 of 2).

```

prm !E1 0.11129
prm !E4 0.25174
prm !burgers = a0/Sqrt(2);
WPPM_Strain_InvariantWilkins(rho , 0.00534, re, 10.93, burgers, 227, E1, E4)

```

Figure 6

Macro call example for macro `WPPM_Strain_InvariantWilkins`.

computer programs

```
def invariantTerm = If (invariantTerm_0 < 0,  
1000, invariantTerm_0)
```

(see Fig. 3). This condition forces the minimization path to exclude the current combination of coefficients but is not directly reflected in the final profile if reflections are weak, which is where controlling the correctness of the line profile may be difficult. It is therefore suggested to control the invariant coefficients resulting from the refinement, and for this reason a supplementary macro (`Out_invariant`; see Fig. 7) was defined, providing values of the invariant coefficients for selected crystallographic directions. The macro requires the user to define a file name for the output, and the input parameters are the space group and the corresponding invariant coefficients. Also in this case macro redefinitions are available for all Laue classes. The following is an example written for the space-group number 227, belonging to the $m\bar{3}m$ Laue class (Table 1):

```
Out_Invariant("CubicInvariant.txt", 227, E1, E4).
```

The macro `WPPM_Strain_InvariantPAH` (Fig. 4), is based on the following definition of microstrain (Scardi *et al.*, 2015; Leonardi & Scardi, 2016):

$$\langle \varepsilon_{hkl}^2(L) \rangle = (d_{hkl}^4/a^4)\Gamma_{hkl}(\alpha/L + \beta). \quad (10)$$

As with the macro `WPPM_Strain_InvariantWilkins`, line broadening anisotropy is accounted for by the invariant Γ_{hkl} , with coefficients α and β to be refined to give the appropriate magnitude of the effect. Note that alternative expressions can be implemented: the reason for using equation (10) is the phenomenological evidence of the Adler & Houska (1979) model, which proved appropriate in many cases (e.g. see Scardi *et al.*, 2015; Leonardi & Scardi, 2015, 2016). The resulting FT expression is

$$A_{hkl}^D(L) = \exp[(-2\pi^2 d_{hkl}^2/a^4)\Gamma_{hkl}(\alpha L + \beta L^2)]. \quad (11)$$

```
macro Out_Invariant(file,sg,E1, E2, E3, E4, E5, E6, E7, E8, E9, E10, E11, E12, E13,  
E14, E15)  
{  
    out file  
        Out_String("\nCell Parameters")  
        Out(Get(a), "\na = %V;")  
        Out(Get(b), "\nb = %V;")  
        Out(Get(c), "\nc = %V")  
        Out(Get(al), "\nalpha = %V;")  
        Out(Get(be), "\nbeta = %V;")  
        Out(Get(ga), "\ngamma = %V")  
  
        Out_String("\n\n/")  
        Out_String("*")  
        Out_String(" H - K - L ----- Inv")  
        Out_String(" *")  
        Out_String("/")  
  
    phase_out file append  
        load out_record out_fmt out_eqn  
    {  
        "\n%4.0f" = H;  
        "%4.0f" = K;  
        "%4.0f" = L;  
        "%12.2f" = getInvariant(sg, E1, E2, E3, E4, E5, E6, E7, E8, E9, E10,  
        E11, E12, E13, E14, E15);  
    }  
}
```

Figure 7
TOPAS macro `Out_Invariant`, providing values of the invariant form for selected crystallographic directions.

```
prm !E1 0.57782  
prm !E4 0.00190  
prm !E7 0.00107  
prm !E13 0.01291  
WPPM_Strain_InvariantPAH( av , 0.5, bv , 0.01, 167, E1, E4, E7, E13)  
Out_Invariant("TrigonalInvariant.txt", 167, E1, E4, E7, E13)
```

Figure 8
Macro call example for macro `WPPM_Strain_InvariantPAH`.

Table 2

TOPAS results of WPPM macros for the sample of Fig. 9 (s.u. on the least significant digits in parentheses).

Mean domain size, $\langle D \rangle$, standard deviation of the distribution of Fig. 9(b), s.d., average dislocation density, ρ , effective outer cut-off radius, R_e , and dislocation character (edge fraction), f_E . The table also lists unit-cell parameter, a_o , Debye–Waller coefficients, B_{ISO} , and amount of MgO contaminant phase.

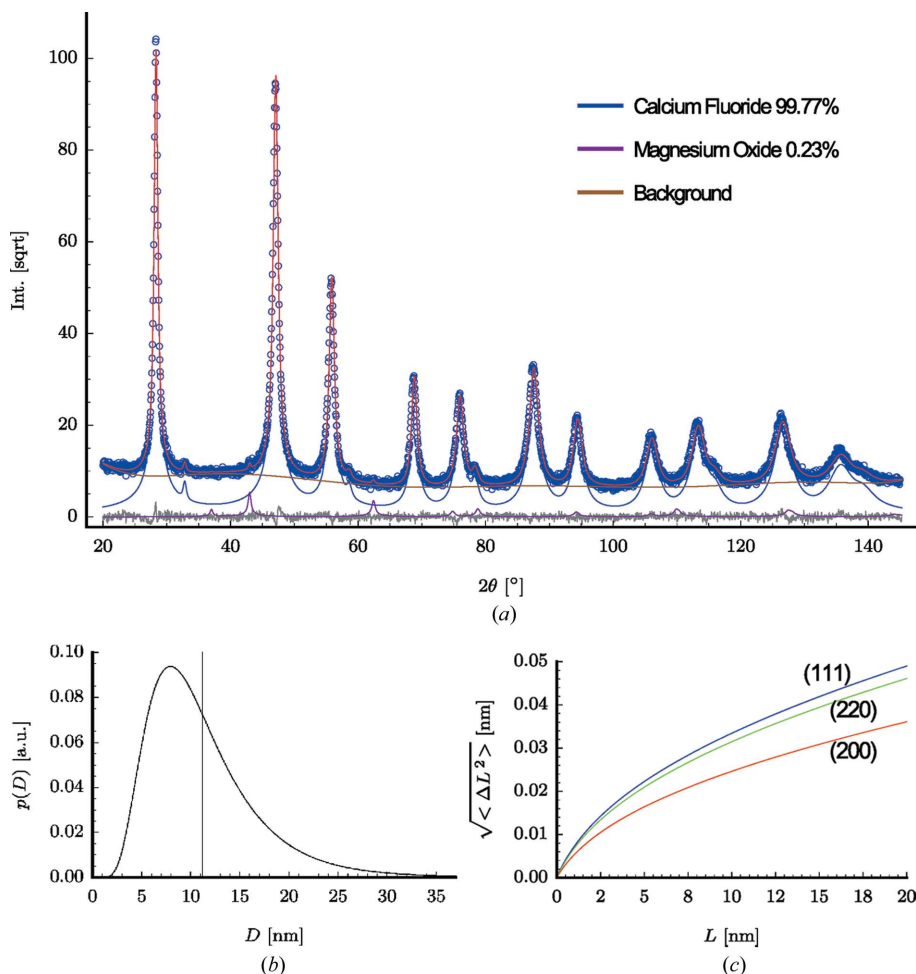
$\langle D \rangle$	s.d. (nm)	$\rho (\times 10^{16} \text{ m}^2)$	R_e (nm)	f_E	a_o (nm)	$B_{\text{ISO}}(\text{Ca}^{+2}) (\text{\AA}^2)$	$B_{\text{ISO}}(\text{F}^{-}) (\text{\AA}^2)$	MgO
11.2 (4)	5.7 (3)	1.02 (1)	2.9 (3)	0.7 (7)	0.54616 (25)	0.601 (17)	0.966 (25)	0.23 (6)

This expression is equivalent to the FT of a convolution of a Lorentzian (related to the αL term in parentheses) with a Gaussian (related to the βL^2 term) function, that is, a Voigt profile function, with line broadening anisotropy represented by Γ_{hkl} . As with the previous macro, it is suggested to limit the variability range of the parameters. Users are required to provide the space group and invariant coefficients; starting values may be those calculated for dislocation line broadening, or just real numbers. The example in Fig. 8 is for a phase belonging to the trigonal system.

3. Examples of applications

As shown recently (Abdellatif *et al.*, 2013*a,b*), high-energy milling of fluorite can reduce the crystalline domains to nanometric dimensions and introduce a high density of dislocations. The diffraction line profiles are therefore affected by size and strain broadening, the latter caused in large part by the line defects. Fig. 9(a) shows *TOPAS* results for a fluorite powder ground for 32 h in a Fritsch P4 planetary mill (Broseghini *et al.*, 2016). The macro `WPPM_Strain_InvariantWilkens` was used with the invariant coefficients known for the primary dislocation slip system of fluorite (Abdellatif *et al.*, 2013*b*), together with the macro `WPPM_Sphere_LogNormDIST` for size broadening. The instrumental profile was previously determined using a standard LaB₆ powder (NIST SRM 660b; Cline *et al.*, 2010) and the fundamental parameters approach of *TOPAS* (see Coelho, 2018, and references therein). Modelling results are summarized in Table 2. With the two macros we obtain the mean and standard deviation of the distribution of diameters (spherical domains), shown in Fig. 9(b), the mean dislocation density, the effective outer cut-off radius, and the character of the dislocation [f_E , defined in the range from 0 (screw) to 1 (edge)], in addition to the usual refinement parameters: unit-cell parameter and Debye–Waller coefficients in this case. The fit also included MgO, present as a contaminant of the starting material.

The microstrain results can also be represented graphically in terms of Warren plots, $(\Delta L_{hkl}(L))^{1/2} = [\langle \varepsilon_{hkl}^2(L) \rangle^{1/2} L]$ versus L , assuming $\langle \Delta L_{hkl}(L) \rangle = 0$ for all hkl and L (Warren & Averbach, 1950). This is the trend of the standard deviation of the distribution of atomic displacements over a distance L within the crystalline domain, along the given $[hkl]$ direction of the scattering vector. As recently pointed out by some of the authors (Rebuffi *et al.*, 2016; Scardi *et al.*, 2018), Warren plots have the advantage of describing the microstrain

**Figure 9**

TOPAS results for a ball-milled fluorite powder (Fritsch P4 mill, operated for 32 h at $\Omega = 200 \text{ r min}^{-1}$, main disc/jar coupling $\omega/\Omega + 1 = -2.6$). (a) The powder pattern was collected in Bragg–Brentano geometry (Rigaku PMG/VH), using Cu K α radiation. (b) Domain size (diameter, D) distribution with mean valued $\langle D \rangle$ (vertical line). (c) Warren plot for (111) (blue), (220) (green) and (200) (red) directions. See text, Broseghini *et al.* (2016) and Broseghini (2017) for details. The coefficients of the invariant form of equation (8) are taken from Abdellatif *et al.* (2013*a,b*). In these papers the coefficients given by A and B are related to those of equation (9) as $E_1 = A$ and $E_2 = A + B/2$ (Scardi & Leoni, 1999).

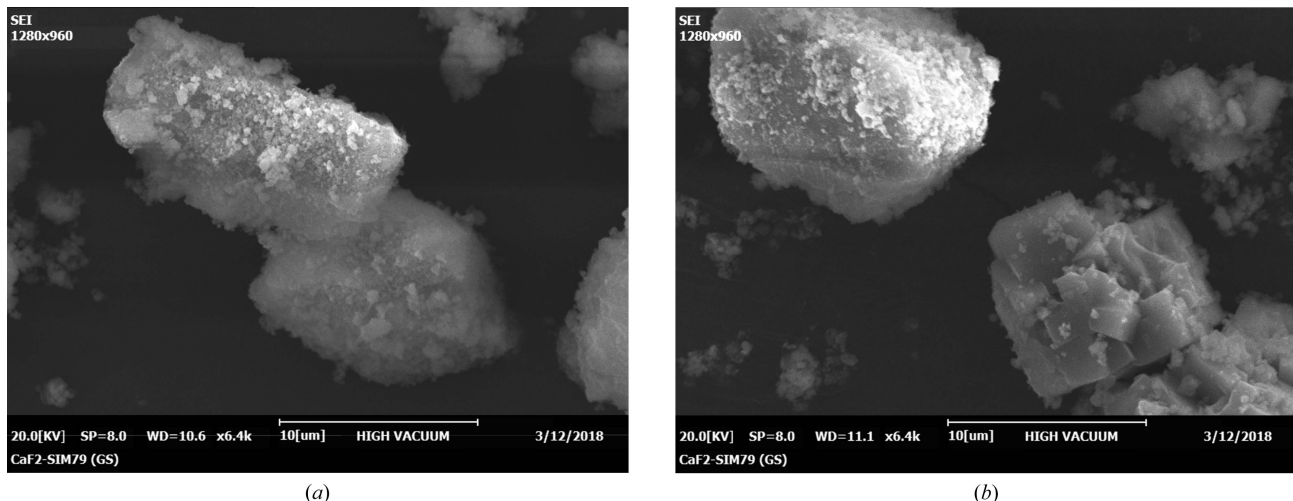


Figure 10

SEM micrographs of (a) the homogeneously ground fluorite milled in a standard cylindrical jar (Fig. 9) and (b) the powder ground in a 3-lifter jar (Fig. 11).

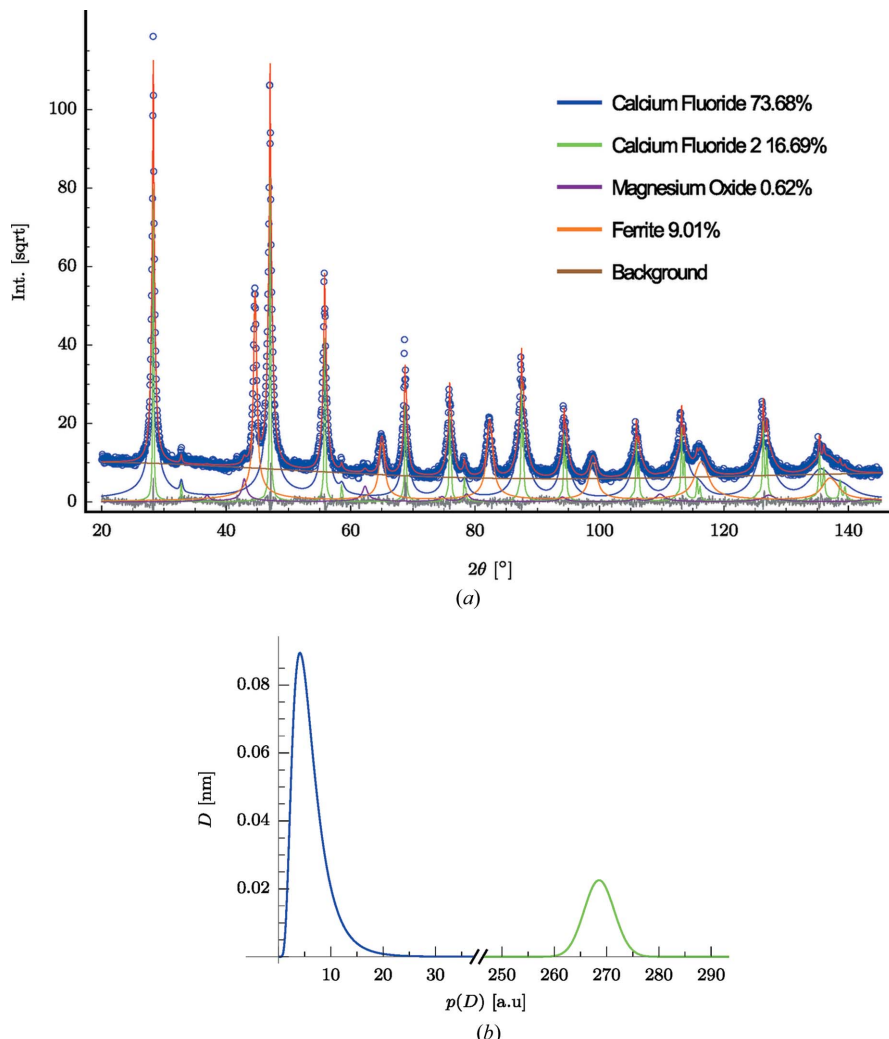


Figure 11

TOPAS results for a fluorite sample ground in a jar of new design (3-lifter jar, 32 h at $\Omega = 200 \text{ r min}^{-1}$, main disc/jar coupling $\omega/\Omega + 1 = -3.0$; Broseghini, 2017). (a) The powder pattern was modelled by assuming two separate fluorite fractions, respectively, nanocrystalline and sub-microcrystalline, with MgO and ferritic steel as contaminants. (b) The size distribution of the two fluorite fractions: fine fraction (blue) and coarse fraction (green).

effect without committing to one specific source, for example dislocations in this case. As shown in Fig. 9(c), the trend changes with the crystallographic direction, with a broadening effect larger along $[hhh]$ than $[h00]$. This result reflects the nature of the elastic behaviour of CaF_2 which, like several isomorphous binary compounds, has soft and stiff directions, respectively, along $[hhh]$ and $[h00]$ (Abdellatif *et al.*, 2013*a,b*). If we think in terms of a microstrain attributed entirely, or in large part, to dislocations, the resulting density is quite high ($1 \times 10^{16} \text{ m}^{-2}$), while R_e (2.9 nm) is smaller than the domain size, so that the Wilkens parameter (Wilkens, 1970) $R_e(\rho)^{1/2} = 0.3$. A value below one indicates strongly interacting dislocations, as in dipoles, domain walls and boundary regions, as pointed out in other studies on finely ground fluorite (Abdellatif *et al.*, 2013*a,b*; De Giudici *et al.*, 2005).

Note that the use of the two macros, besides providing the microstructural information discussed so far, leads to better modelling results, with statistical indices ($R_{wp} = 7.10\%$, GoF = 1.15) about 10% lower than those obtained using the standard double-Voigt profile model of TOPAS (Coelho, 2017, 2018).

The refinement procedure is quite robust. This is appreciated in the case of a powder ground in non-optimized conditions in a new-design jar (Broseghini, 2017). As shown in the

micrographs of Fig. 10, while the former sample is uniformly made of aggregates of much smaller particles (*a*), the use of a jar with a 3-lifter design under not optimized milling conditions leaves a fraction of little or not-ground fluorite (*b*). *TOPAS* modelling of the powder pattern with the two macros can be used successfully again. As shown in Fig. 11, we can model the data by considering two separate fractions of fluorite, so as to determine the relative percentage, also

considering the MgO traces and the additional contamination from the steel balls and jar [body-centred cubic (b.c.c.) iron phase]. Details of this study of newly conceived jars and process optimization can be found elsewhere (Broseghini, 2017), but it is here interesting to show the resulting bimodal size distribution of fluorite (Fig. 11*b*).

The next application concerns ball-milled CaCO_3 . The pristine powder was made of calcite (hexagonal, space group 167), but the extensive (64 h) high-energy grinding caused a partial transformation to aragonite (orthorhombic, space group 62) (Pesenti *et al.*, 2008). Quartz is present as contaminant of the starting materials, whereas b.c.c. iron comes also in this case from the milling vials.

The powder pattern shows broad peak profiles for both polymorphs, with increasing broadening with the 2θ angle, clearly revealing a relevant domain size and microstrain effect (Fig. 12*a*) typical of heavily ground materials. Transmission electron microscopy (TEM) shows strongly agglomerated clusters of nanocrystalline domains (Fig. 12*b*). Differently from fluorite, where a reasonable assumption that dislocations were the main source of microstrain was possible, here no clear indication emerges. Previous work has shown that none of the known slip systems gives a line broadening fully matching the experimental pattern of ball-milled CaCO_3 (Pesenti, 2007; Pesenti *et al.*, 2008), although the presence of some defects in the fine (nanoscale) domains is clearly observed in the polycrystalline aggregates of ball-milled CaCO_3 (Pesenti, 2007). In this condition it is likely that more mechanisms, still to be clarified, contribute to the microstrain, so that it is convenient to use the macro WPPM_Strain_InvariantPAH. Modelling results are shown in Fig. 12(*a*), using the macro with the number of refinable invariant coefficients corresponding to the space-group number of each polymorph (respectively, 3 and 6 for calcite and aragonite; Table 1), together with the size broadening macro with refinable μ and σ . The results show an improvement of statistical quality of about 5% with respect to the standard double-Voigt profile model of *TOPAS* (Coelho, 2017, 2018) and provide the microstructural information shown in Fig. 12(*c*), as

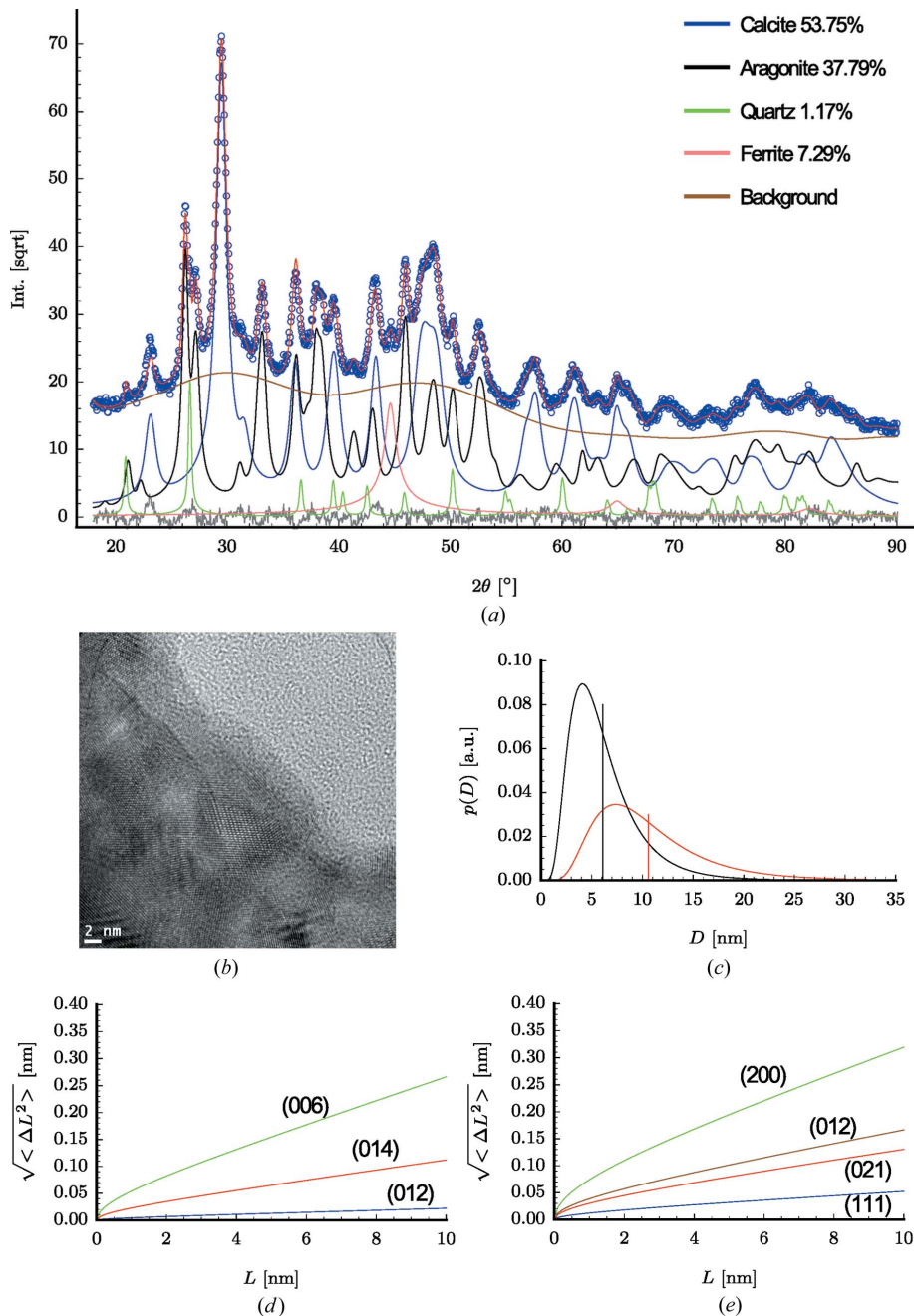


Figure 12
TOPAS results for a ball-milled CaCO_3 powder [Fritsch P4 mill, 64 h; details reported by Pesenti *et al.* (2008)]. (*a*) The pattern is modelled by assuming the presence of calcite, aragonite, quartz and b.c.c. iron: phase percentages are shown in the inset. (*b*) TEM micrograph of the ball-milled powder; (*c*) domain size distribution of the two CaCO_3 polymorphs (red – aragonite; black – calcite), with indication of the corresponding mean sizes (bars); and Warren plots for (*d*) calcite and (*e*) aragonite for a selection of Bragg peaks.

computer programs

distribution of domain size, and Figs. 12(*d*) and 12(*e*), as Warren plots for each polymorph. The latter show the anisotropy of the strain broadening effect, quite relevant in both polymorphs.

4. Simulation of the surface relaxation in nanocrystals

The generality of the approach described so far is such as to include non-routine cases, like atomistic simulations of nanocrystal powders. The atomic coordination of free surfaces

```
macro WPPM_SR_Sphere(sigmac, sigmav, betac, betav, roc, rov, radioc, radiov,
shiftc, shiftv, s11, s12, s44)
{
    #m_argu sigmac 'in TPa if s11, s12, s44 are in TPa^-1
    #m_argu betac 'in nm
    #m_argu roc 'in nm
    #m_argu radioc 'in nm
    #m_argu shiftc 'pure number

    WPPM_ft_conv =
    {
        def sigma = CeV(sigmac,sigmav);
        def beta = CeV(betac,betav);
        def ro = CeV(roc, rov);
        def RR = CeV(radioc, radiov);
        def shift = CeV(shiftc, shiftv);
        def qhkl = 2*Pi/(D_spacing*0.1); 'we need interplanar distance in nm

        def deltaL = meanDeltaL(RR, WPPM_L/(shift+1), H, K, L, s11, s12, s44,
sigma, beta, ro);
        def deltaLsquare = meanDeltaL2(RR, WPPM_L/(shift+1), H, K, L, s11, s12,
s44, sigma, beta, ro);

        def deltaLsquareCorr = deltaLsquareCorrFun(deltaL, deltaLsquare, shift,
WPPM_L/(shift+1));

        return Exp((-1/2)*qhkl^2*deltaLsquareCorr);
    }

    WPPM_ft_conv_im =
    {
        def sigma = CeV(sigmac,sigmav);
        def beta = CeV(betac,betav);
        def ro = CeV(roc, rov);
        def RR = CeV(radioc, radiov);
        def shift = CeV(shiftc, shiftv);
        def qhkl = 2*Pi/(D_spacing*0.1); 'we need interplanar distance in nm

        def deltaL = meanDeltaL(RR, WPPM_L/(shift+1), H, K, L, s11, s12, s44,
sigma, beta, ro);

        def deltaLCorr = deltaLCorrFun(deltaL, shift, WPPM_L/(shift+1));

        return qhkl*deltaLCorr;
    }

    WPPM_L_max = 2*CeV(radioc, radiov);
    WPPM_th2_range = 55;
}
```

Figure 13

TOPAS macro `WPPM_SR_Sphere`, a microstrain line broadening model for the surface relaxation in a monodisperse spherical nanocrystal. Note that, differently from the previous macros, *TOPAS* is set to perform the FT up to the particle diameter as maximum Fourier length: `WPPM_L_max = 2*CeV(radioc, radiov)`. No stopping criterion is based on the values of the real or imaginary FT (the command `WPPM_brake_on_small` is not used). This is because in this case the real and imaginary strain FT components may be non-monotonic. For the exact definition of the functions `meanDeltaL`, `meanDeltaL2` and so forth, see the supplementary information.

(surface relaxation effect) induces an inhomogeneous strain in nanocrystals, with a corresponding line broadening in the powder diffraction pattern (Scardi *et al.*, 2015).

To study the nature of this effect, a model has been proposed for spherical nanocrystals (Perez-Demydenko & Scardi, 2017), giving an expression for the micro-strain dependent on three main parameters: (i) an effective hydrostatic pressure, σ , (ii) the thickness of the surface region where atoms are displaced because of sub-coordination, r_o , and (iii) the maximum radial displacement of the surface atoms, β :

$$\langle \varepsilon'_{hkl}(L') \rangle L' = a\sigma G_1(R, L') + b\sigma G_2(R, L') + c\sigma G_3(R, L') + \beta G_4(R, L', r_o), \quad (12)$$

$$\begin{aligned} \langle \varepsilon'^2_{hkl}(L') \rangle L'^2 = & a^2 \sigma^2 F_1(R, L') + ab\sigma^2 F_2(R, L') + b^2 \sigma^2 F_3(R, L') \\ & + ac\sigma^2 F_4(R, L') + bc\sigma^2 F_5(R, L') + c^2 \sigma^2 F_6(R, L') \\ & + a\beta\sigma F_7(R, L', r_o) + b\beta\sigma F_8(R, L', r_o) \\ & + c\beta\sigma F_9(R, L', r_o) + \beta^2 F_{10}(R, L', r_o). \end{aligned} \quad (13)$$

The coefficients a , b , c carry the dependence on the elastic properties of the material (s_{11} , s_{12} , s_{44} , elastic constants for a cubic material) and on the Miller indices of the given Bragg peak, *i.e.* account for the anisotropic strain broadening effect. F_i and G_i are known (analytical) functions of the crystalline domain size, R ($= D/2$, spherical domain radius), r_o and the Fourier length, L' [see Perez-Demydenko & Scardi (2017) for details]. In equations (12) and (13) the strain refers to an ideal small crystal, with the nominal unit-cell parameter (a'_o) of the bulk material. In practical uses the strain must refer to the same structure but with the average unit-cell parameter a_o (Warren, 1990). It can be shown that using equations (12) and (13) this would read as

$$\langle \varepsilon_{hkl}(L) \rangle = \frac{a'_o}{a_o} \left[\langle \varepsilon'_{hkl}(L') \rangle - \left(\frac{a'_o}{a_o} - 1 \right) \right], \quad (14)$$

$$\begin{aligned} \langle \varepsilon^2_{hkl}(L) \rangle = & \left(\frac{a'_o}{a_o} \right)^2 \left[\langle \varepsilon'^2_{hkl}(L') \rangle - 2\langle \varepsilon'_{hkl}(L') \rangle \left(\frac{a'_o}{a_o} - 1 \right) \right. \\ & \left. + \left(\frac{a'_o}{a_o} - 1 \right)^2 \right], \end{aligned} \quad (15)$$

where $L = (a_o/a'_o)L'$ and L' covers the un-relaxed, or as-built, atomic configuration (see the supplementary information for details).

As with the other microstrain macros, equation (15) can be used in equation (6) to model the corresponding strain broadening effect. However, in this case there is a non-zero L -dependent mean strain [equation (14)], so that the Fourier transform of the strain broadening D component of the line profile is complex, $A_{hkl}^D(L) + iB_{hkl}^D$ (Warren, 1990), with an

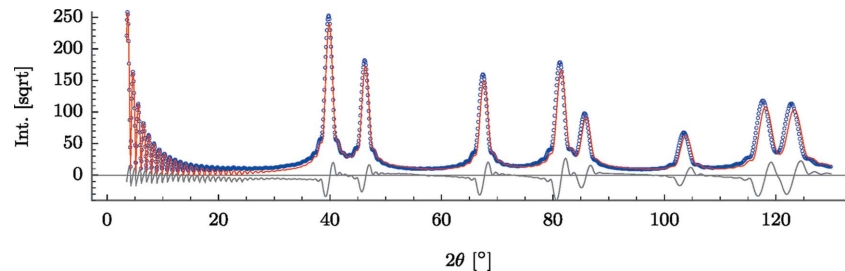


Figure 14

Comparison between the diffraction pattern of a spherical Pt nanoparticle of radius 4.71 nm carved from an infinite crystal structure (blue dots) and the pattern simulated by TOPAS using the WPPM_SR_Sphere macro (red line). The unit-cell parameter used for the latter was 3.9115 Å, obtained by refining the pattern of the corresponding relaxed particle with constant values of the model parameters (see Fig. 16) $\sigma = 3.92 \times 10^{-1}$ GPa, $\beta = 2.14 \times 10^{-1}$ Å and $r_o = 1.33$ Å in TOPAS.

imaginary component that can be approximated as (Perez-Demydenko & Scardi, 2017)

$$B_{hkl}^D(L) = (2\pi/d_{hkl})L\langle \varepsilon_{hkl}(L) \rangle. \quad (16)$$

This model has been implemented in the macro WPPM_SR_Sphere(*, sigma, beta, ro, R, k, s11, s12, s44*) shown in Fig. 13 (full details in the supplementary information²). The refinable parameters are *sigma* (σ), *beta* (β) and *ro* (r_o); *R* is the radius of the spherical domain and *k* the ratio between the unit-cell parameter refined on the experimental data and that of the ideal bulk phase [a_o/a'_o in equations (14) and (15)]. The elastic constants are fixed for the studied cubic phase. Fig. 14 shows the application of the new macro to simulating the powder pattern of a system of relaxed spherical nanocrystals. This case study refers to Pt nanocrystals of radius 4.71 nm and 28 867 atoms. Given the atomic coordinates, the Debye scattering equation was used to simulate the powder pattern shown by blue dots in Fig. 14. The surface relaxation effect is obtained by adding the WPPM_SR_Sphere macro. This is shown as a full line in Fig. 14, obtained using parameters σ , β and r_o from Table 1 of Perez-Demydenko & Scardi (2017) with the input file in Fig. 15.

A striking feature of the surface relaxation effect is the atomic displacement across the nanoparticle. This can be represented as in Fig. 16, showing the mean radial displacement. Data points (blue dots) are given by a molecular dynamics (MD) simulation made using LAMMPS (Plimpton, 1995), with an embedded atom method potential under NVE conditions [constant number of atoms, volume and energy: see Perez-Demydenko & Scardi (2017) for details]. The full line corresponds to the surface relaxation model with the parameters σ , β and r_o used to run the macro.

As shown in Fig. 14, the main effect of the SR model (full line) is to shift the Bragg peaks to higher angles than those of the starting perfect nanocrystals, as an effect of the average

² This macro is supplied in the separate file WPPM_SR_Sphere_macro.inc of the supplementary information. In order to use it, copy the file into the folder where you keep the input file and add the command #include WPPM_SR_Sphere_macro.inc.

computer programs

```
prm !s11 = 7.33706; 'elastic costants for Pt in TPa^-1 units
prm !s12 = -3.0796;
prm !s44 = 12.987;

prm RRR 4.67813` min .001 max = Min(2 Val+.01,20); val_on_continue=Rand(0, 4); 'nm
prm nofAtoms 28727.79819`
fit_obj = sxs(X, 10*RRR /*A*/, 1.54059/*A*/, nofAtoms, 78);
prm !aPtbulk = 3.9242;
STR(F_M_3_M)
phase_name "platinum"
Cubic(!aPt 3.9115_0.000041)
site Pt x 0 y 0 z 0 occ Pt 1 beq 0
MVW( 780.312, 59.845, 100.000`)

prm !ssigma -0.000392 ' TPa
prm !bbeta -0.0214 ' nm
prm !rro 0.133 ' nm

prm kk = Constant(aPt)/aPtbulk -1;
WPPM_Sphere(, RRR)
WPPM_SR_Sphere(,ssigma,,bbeta,,rro,,RRR,,kk,s11,s12,s44)
```

Figure 15

Macro call example for macro WPPM_SR_Sphere. The sxs function models the small-angle scattering from a sphere; see the supplementary information for its definition.

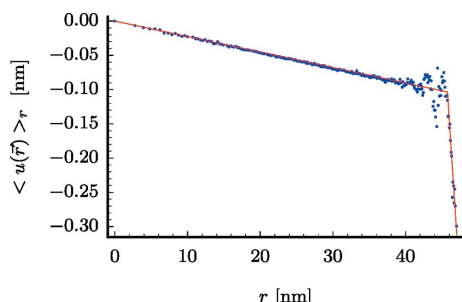


Figure 16

Mean radial displacement component $\langle u(r) \rangle_r$ for atoms at distance r from the nanoparticle centre; the trend is shown for the MD simulation of the relaxed Pt nanoparticle (blue points) and for the surface relaxation model of Perez-Demydenko & Scardi (2017) (red line), using the parameters reported in the caption of Fig. 14. On the basis of the surface relaxation model, it can be shown that $\langle u(r) \rangle_r = (1/5)(3s_{11} + 2s_{12} + s_{44})r\sigma + \beta f_{R, r_o}(r)$ (see the supplementary information).

shrinkage of the Pt nanoparticle correctly engendered by the MD simulation. Additional, finer effects can be observed on peak shape and broadening, which encode the effect of the atomic displacement in the powder pattern.

5. Conclusions

The whole powder pattern modelling approach fits well in the algorithm underlying TOPAS. Indeed, WPPM is based on a convolution of effects, here domain size and microstrain, as in the standard TOPAS modelling of the instrumental profile, based on the fundamental parameter approach. Specific macros have been introduced to deal with (i) the size broadening effect of a system of spherical domains with lognormally distributed diameters; the microstrain broadening effect of dislocations according to (ii) the Krivoglaz–Wilkins theory

and (iii) a general microstrain model, called PAH, thought to flexibly apply to most cases where an inhomogeneous strain has visible and anisotropic effects on the line profile; and finally (iv) a new model of microstrain to describe the surface relaxation effect observed in spherical nanocrystals. The latter is characterized by a complex Fourier transform of the line profile, which allows for naturally modelling peak asymmetry with the whole powder pattern modelling approach. The macros, shown in Figs. 1, 3–5, 7 and 13, will be supported by TOPAS 7.0 and subsequent versions.

References

- Abdellatif, M., Abele, M., Leoni, M. & Scardi, P. (2013a). *J. Appl. Cryst.* **46**, 1049–1057.
- Abdellatif, M., Abele, M., Leoni, M. & Scardi, P. (2013b). *Thin Solid Films*, **530**, 44–48.
- Adler, T. & Houska, C. R. (1979). *J. Appl. Phys.* **50**, 3282–3287.
- Armstrong, N., Leoni, M. & Scardi, P. (2006). *Z. Kristallogr. Suppl.* **23**, 81–86.
- Broseghini, M. (2017). PhD thesis, University of Trento, Italy.
- Broseghini, M., D'Incau, M., Gelisio, L., Pugno, N. & Scardi, P. (2016). *Mater. Des.* **110**, 365–374.
- Cline, J. P., Deslattes, R. D., Staudenmann, J., Kessler, E. G., Hudson, L. T., Henins, A. & Cheary, R. W. (2010). NIST SRM 660b. National Institute of Standards and Technology, Gaithersburg, MD, USA.
- Coelho, A. A. (2017). *TOPAS-Academic*. Version 7. <http://www.topas-academic.net/>.
- Coelho, A. A. (2018). *J. Appl. Cryst.* **51**, 210–218.
- De Giudici, G., Biddau, R., D'Incau, M., Leoni, M. & Scardi, P. (2005). *Geochim. Cosmochim. Acta*, **69**, 4073–4083.
- Dragomir, I. C. & Ungár, T. (2002). *Powder Diffr.* **17**, 104–111.
- Krivoglaz, M. A., Martynenko, O. V. & Ryaboshapka, K. P. (1983). *Fiz. Met. Metallovid.* **55**, 1–12.
- Krivoglaz, M. A. & Ryaboshapka, K. P. (1963). *Fiz. Met. Metallovid.* **15**, 18–31.

- Kužel, R. & Klimanek, P. (1988). *J. Appl. Cryst.* **21**, 363–368.
- Langford, J. I., Louër, D. & Scardi, P. (2000). *J. Appl. Cryst.* **33**, 964–974.
- Leonardi, A., Leoni, M., Siboni, S. & Scardi, P. (2012). *J. Appl. Cryst.* **45**, 1162–1172.
- Leonardi, A. & Scardi, P. (2015). *Front. Mater.* **1**, 37.
- Leonardi, A. & Scardi, P. (2016). *Metall. Mater. Trans. A*, **47**, 5722–5732.
- Martinez-Garcia, J., Leoni, M. & Scardi, P. (2009). *Acta Cryst. A* **65**, 109–119.
- McCusker, L. B., Von Dreele, R. B., Cox, D. E., Louër, D. & Scardi, P. (1999). *J. Appl. Cryst.* **32**, 36–50.
- Mittemeijer, E. & Scardi, P. (2003). *Diffraction Analysis of the Microstructure of Materials*. Springer Series in Materials Science. Berlin, Heidelberg: Springer.
- Perez-Demydenko, C. & Scardi, P. (2017). *Philos. Mag.* **97**, 2317–2346.
- Pesenti, H. (2007). PhD thesis, University of Trento, Italy.
- Pesenti, H., Leoni, M. & Scardi, P. (2008). *Z. Kristallogr. Suppl.* **27**, 143–150.
- Plimpton, S. (1995). *J. Comput. Phys.* **117**, 1–19.
- Popa, N. C. (1998). *J. Appl. Cryst.* **31**, 176–180.
- Rebuffi, L., Troian, A., Ciancio, R., Carlino, E., Amimi, A., Leonardi, A. & Scardi, P. (2016). *Sci. Rep.* **6**, 20712.
- Rietveld, H. M. (1967). *Acta Cryst.* **22**, 151–152.
- Rietveld, H. M. (1969). *J. Appl. Cryst.* **2**, 65–71.
- Scardi, P. (2008). *Microstructural Properties: Lattice Defects and Domain Size Effects*, pp. 376–413. Cambridge: Royal Society of Chemistry.
- Scardi, P., Ermrich, M., Fitch, A., Huang, E.-W., Jardin, R., Kuzel, R., Leineweber, A., Mendoza Cuevas, A., Misture, S. T., Rebuffi, L. & Schimpf, C. (2018). *J. Appl. Cryst.* **51**, 831–843.
- Scardi, P., Leonardi, A., Gelisio, L., Suchomel, M. R., Snead, B. T., Sheehan, M. K. & Tsung, C. K. (2015). *Phys. Rev. B*, **91**, 155414.
- Scardi, P. & Leoni, M. (1999). *J. Appl. Cryst.* **32**, 671–682.
- Scardi, P. & Leoni, M. (2001). *Acta Cryst. A* **57**, 604–613.
- Snyder, R., Fiala, J. & Bunge, H. (1999). *Defect and Microstructure Analysis by Diffraction*. IUCr Monographs on Crystallography. Oxford University Press.
- Stokes, A. & Wilson, A. (1944). *Math. Proc. Camb. Philos. Soc.* **40**, 197–198.
- Ungár, T., Dragomir, I., Révész, Á. & Borbély, A. (1999). *J. Appl. Cryst.* **32**, 992–1002.
- Warren, B. E. (1990). *X-ray Diffraction*. New York: Dover.
- Warren, B. & Averbach, B. (1950). *J. Appl. Phys.* **21**, 595–599.
- Wilkins, M. (1969a). *Fundamental Aspects of Dislocation Theory: Conference Proceedings, National Bureau of Standards, 21–25 April 1969*, edited by J. A. Simmons, R. de Witt & R. Bullough, pp. 1191–1193. US Department of Commerce, National Bureau of Standards, Special Publication 317. Washington, DC: US National Bureau of Standards.
- Wilkins, M. (1969b). *Fundamental Aspects of Dislocation Theory: Conference Proceedings, National Bureau of Standards, April 21–25, 1969*, edited by J. A. Simmons, R. de Witt & R. Bullough, pp. 1195–1221. US Department of Commerce, National Bureau of Standards, Special Publication 317. Washington, DC: US National Bureau of Standards.
- Wilkins, M. (1970). *Phys. Status Solidi (A)*, **2**, 359–370.
- Wilson, A. (1962). *X-ray Optics: the Diffraction of X-rays by Finite and Imperfect Crystals*. Methuen's Monographs on Physical Subjects. London: Methuen.
- Young, R. (1995). *The Rietveld Method*. IUCr Monographs on Crystallography. Oxford University Press.